Journal of Heat and Mass Transfer Research

Journal homepage: http://jhmtr.semnan.ac.ir

Semnan University

# An Axisymmetric Lattice Boltzmann Method Simulation of Forced Convection Heat Transfer for Water/Aluminum Oxide Nanofluid through a Tube under Constant Heat Flux on Wall

**Reza Bahoosh*[,a], Reza Khalili [b], Amin Reza Noghrehabadi[a], Mohammad Jokari [b]**

[a] *Department of Mechanical Engineering Shahid Chamran University of Ahvaz, Ahvaz, Iran.*
[b] *Department of Mechanical Engineering Shahid Chamran University of Ahvaz, Ahvaz, Iran.*

**PAPER INFO**

***Paper history:***
Received: 2020-11-02
Revised: 2021-04-21
Accepted: 2021-04-26

***Keywords:***
Heat transfer;
Constant Heat Flux;
Tube;
ALBM;
Nanofluid.

**ABSTRACT**

Effects of different volumetric fractions and Reynolds number on forced convection heat transfer through water/aluminum oxide nanofluid in a horizontal tube are investigated. The flow regime is laminar and the method of simulation is the axisymmetric lattice Boltzmann method (ALBM). The profiles of velocity and temperature were uniform at the input section, on the tube walls the uniform heat flux was considered; moreover, hydrodynamic, and thermal development conditions at the output section were applied. It was observed that an increase in the volumetric concentration of the nanoparticles added to the forced convection heat transfer coefficient and Nusselt number of the nanofluid, as compared to the base fluid. For a volumetric fraction of 5% and Reynolds number of 100 at the input section of the tube ($0.1 \leq \frac{X}{D} \leq 7$) the forced convection heat transfer coefficient increased by 24.165%, while an average increase of 21.361% was observed along the entire length of the tube ($0 \leq \frac{x}{D} \leq 30$). A comparison between the improvements in heat transfer at the two input temperatures, it was found that the forced convection heat transfer coefficient and Nusselt number will increase further at the lower input temperature; Moreover, with increasing Reynolds number, the percent improvements in forced convention heat transfer coefficient and Nusselt number increased.

DOI: 10.22075/JHMTR.2021.21718.1312



## 1. Introduction

This Researchers' recent efforts toward enhancing heat transfer has led to the invention of different methodologies for such purpose [1]. The paramount importance of heat transfer in various industries has always been a cause for improving heat transfer methods and optimizing them for industrial contexts. Poor heat transfer properties of typical fluids represent the first serious barrier against enhancing the efficiency of heat exchangers. The developments in nanotechnology during the past two decades and the application of nanofluids as a heat transfer agent have provided researchers with new approaches [2].

Eastman et al. [3] measured the thermal conductivity of nanofluids by evaluating aluminum oxide, copper and copper oxide nanoparticles in water and oil. In their study, they observed a 60% increase in thermal conductivity upon adding the nanoparticles up to 5%. In another work [4], they used copper nanoparticles of smaller than 10 nm in diameter, ending up with a 40% increase in thermal conductivity of ethylene glycol at a nanoparticle concentration of 0.3%. They attributed such an increase mainly to the large surface-area-to-volume ratio of the nanoparticles. Assuming that a nanofluid largely mimics the behavior of an equivalent single-phase fluid rather than a liquid-solid mixture, Xuan and Roetzel [5] proposed two different methods for developing relationships for predicting heat transfer through nanofluid. According to the assumption made by Xuan and Roetzel, in absence of any slipping velocity in between the continuous phase (liquid) and discrete phase (the nanoparticles dispersed across the liquid) and upon an establishment of thermodynamic equilibrium between the nanoparticles and the liquid, the resultant nanofluid can be deemed a

* *Corresponding Author: Reza Bahoosh, A faculty member of the Mechanical Department of the Shahid Chamran University of Ahvaz, Ahvaz, Iran.*
Email: bahoosh@scu.ac.ir

pure (single-phase) fluid. Following a second approach, Xuan and Roetzel focused on the random particle motions under the effect of Brownian forces, friction, and gravity and proposed a dispersion model for considering the impact of thermal dispersion.

Wen and Ding [6] experimentally investigated forced convection heat transfer through the water/$Al_2O_3$ nanofluid in a copper-made tube under laminar flow. Results of the experiments performed by these researchers showed a superior increase in forced convection heat transfer through the nanofluid rather than the base fluid; moreover, the increase was even more pronounced in the input section of the tube and somewhat decreased as one moved along the axis of the tube. Accordingly, it was suggested that the thermal entrance length of the nanofluid is larger than that of the base fluid, and this length increases with increasing nanoparticle concentration. Furthermore, observations indicated increased heat transfer through the nanofluid with increasing Reynolds number and the volumetric fraction of the nanoparticles. They further figured out that the then-existing equations (Shah's equation [7]) could not be applied for predicting forced convection heat transfer through nanofluids along the input section of a tube. They referred to particle migration and disorders in the boundary layer (reduced thickness of the boundary layer) as the main causes of the enhanced heat transfer. Noghrehabadi and Pourrajab [8] experimentally investigated the forced convection heat transfer coefficient and Nusselt number through water-$Al_2O_3$ nanofluid in a circular tube under fixed-heat transfer boundary conditions. For this purpose, they utilized aluminum oxide nanoparticles with an average diameter of 20 nm and calculated the heat transfer coefficient of the nanofluid at different Reynolds numbers ranging from 1057 to 2070 for three volumetric fractions: 0.1%, 0.3%, and 0.9%. A review of the results showed that the forced convection heat transfer coefficient and Nusselt number of the nanofluid were higher than those of the base fluid with the highest increase in heat transfer (~16.8%) observed at a volumetric fraction of 0.9% and a Reynolds number of 2070. In addition, it was found that the number of increases in forced convection heat transfer coefficient and Nusselt number are functions of the volumetric fraction of the nanoparticles. Fitting a curve to their experimental data, they developed a mathematical model for estimating the Nusselt number. The model provided good accuracy against the respective experimental data.

Hassan-Zadeh *et al*. [9] conducted a three-dimensional study on forced convection heat transfer through water/$Al_2O_3$ nanofluid in a tube with a laminar flow regime with the use of the finite-volume method and considered a fully developed velocity profile at the input section of the tube. Simulations were performed for a wide range of volumetric fractions of the nanoparticles for two different nanoparticle sizes. The results indicated that the incorporation of $Al_2O_3$ nanoparticles into the base fluid enhanced the rate of growth of the thermal boundary layer and that this growth is a function of the volumetric concentration and size of the nanoparticles.

Most of the numerical research on nanofluids, including those cited above, have been performed using such methods as finite-volume and finite-difference methodologies. In recent years, following a statistical mechanics-based approach and being derived from the kinetic theory of gases [10], the Lattice Boltzmann method has gained great deals of attention among researchers. Since the present research is grounded in the Lattice Boltzmann method, a brief description of the research works wherein such a method has been used is presented in the following.

Considering the external and internal forces affecting suspended nanoparticles and the nanoparticle-fluid interactions, Xuan and Yao [11] proposed a Lattice Boltzmann model for simulating the processes of flow and energy transfer through nanofluids. In their study, they emphasized the irregular motion of the nanoparticles and calculated the distribution of the suspended nanoparticles in the nanofluid using a series of forces. Based on their findings, the Brownian force was the dominant factor affecting the random convection and accumulation of nanoparticles. Kefayati *et al.* [12] utilized the Lattice Boltzmann methodology for examining free heat transfer through water-silicon dioxide in tall vessels. Their experiments targeted different volumetric fractions ranging between 0 and 4 for Rayleigh numbers from $10^3$ to $10^5$. They showed that, at all of the studied Rayleigh numbers and for all ratios of the rectangular vessel, the presence of nanofluid enhanced the Nusselt number over that of the base fluid. Servati et al [13] studied the impact of magnetic field on forced convection flow of a nanofluid in a channel that is filled with porous media by use of LBM. They concluded that by increasing the volume fractions of AL2O3, the outlet temperature and velocity at the outlet of the channel, and also the Nusslet number showed a significant increase. Sidik and Mamat [14] reported comprehensive research on recent developments and research works on simulating the flow and heat transfer of nanofluids by the use of the Lattice Boltzmann method. In this comprehensive study, numerous research works were reviewed on different geometries, different nanoparticles, laminar and turbulent flow regimes, and convection heat transfer (free, forced, and mixed) with single-phase and two-phase models for nanofluids. Cheng et al. [15] utilized the lattice Boltzmann method implemented on compute unified device architecture-enabled graphical processing unit to investigate the multiphase fluid pipe flow. The vertical and horizontal multiphase pipes flow were simulated and discussed. Goodarzi et al. [16] developed a Nanoscale method of lattice Boltzmann to predict the fluid flow and heat transfer of air through the inclined lid-driven 2-D cavity while a large heat source is considered inside it. Nazari and Kayhani [17] provided a comparative study on natural convection in an open-end cavity using LBM. They simulated the result by applying two different

hydrodynamic and two different thermal boundary conditions (with first and second-order accuracy), which indicated the same Nusselt number in all boundaries. Bahoosh et al. [18] presented a two-dimensional model of a polymer fuel cell. They used LBM to simulate the single-phase fluid flow and mass transfer within the cathode microstructure and investigated the effects of the gas diffusion layer structure (carbon fibers diameters changes) on the reactive gas flow. They showed that the increase in the carbon fibers' diameter causes the uniform distribution of oxygen throughout the gas diffusion layer.

Shomali and Rahmati [19] developed a Cascade LBM method with a non-constant Bosanquet parameter to observe the gas flows in a microchannel. The results of the proposed method showed an improvement in comparison with the classic methods.

As is evident from a review of the above-mentioned pieces of literature, many numerical and experimental works have been done on studying heat transfer through nanofluids in various geometries and boundary conditions for different types of nanofluid. However, to the best of our knowledge, no two-dimensional study has been performed on steady laminar forced convection heat transfer in a tube with fixed heat flux on the walls using the Lattice Boltzmann method. Consequently, in the present work, the axisymmetric lattice Boltzmann method (ALBM) to both the flow part and energy part under fixed heat flux on the walls of the tube are applied; uniform velocity and temperature profiles have been assumed at the input section of the tube, i.e. the flow and temperature develop along the tube. In addition, the effect of input temperature on forced convection heat transfer through the nanofluid was studied.

## 2. Problem description Style

The geometry of the studied problem is demonstrated schematically in Figure 1. It is a tube at a length-to-diameter ratio of $\frac{L}{D} = 30$. The no-slip condition was applied to the wall of the tube, with a fixed heat flux of $q'' = 6000$ w/m$^2$ applied to it. As an incompressible nanofluid, water / $Al_2O_3$ nanofluid was sent into the tube with laminar flow in steady-state and uniform velocity ($u = U_{in}$) and temperature ($T_{in} = 288K$ or $T_{in} = 293K$) at the input section. At the exit, fully developed conditions both hydrodynamically and thermally are applied. Reynolds number of the fluid flowing into the tube was fixed at 50, 75, and 100. The nanoparticles were assumed to be spherical with an average particle diameter of 20 nm. Those were supposed to be in thermodynamic equilibrium with the base fluid with no-slip concerning its molecules.

## 3. Numerical method description

The numerical method that is utilized in this research is explained as follows.

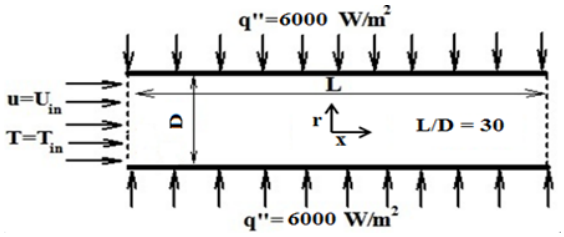


**Figure 1.** Schematics of the problem in a tube.

### *3.1. Axisymmetric lattice Boltzmann method for hydrodynamic part of the flow*

To simulate axisymmetric flows, Zhou [20] revised the so-called general axisymmetric lattice Boltzmann method [21] to eliminate the need for calculating the velocity gradients. The Zhou has modified the Lattice Boltzmann equation with force and source/well terms is as follows:

$$f_\alpha(\vec{x} + \vec{e}_\alpha \Delta t, t + \Delta t) - f_\alpha(\vec{x}, t) = -\omega_h\left[f_\alpha(\vec{x}, t) - f_\alpha^{eq}(\vec{x}, t)\right] + w_\alpha \theta\, \Delta t + \frac{\Delta t}{\kappa c^2} e_{\alpha i} F_i \quad (1)$$

Where $f_\alpha$ and $f_\alpha^{eq}$ are the particle and the local equilibrium distribution function respectively. $\Delta t$, $\vec{x}$, $w_\alpha$ and $\theta$ are the time step, a coordinate vector, a series of weighting factors and the source or sink term as per respectively.

$$\theta = -\frac{\rho u_r}{r} \quad (2)$$

Moreover, $F_i$ is the force term with its definition expressed as follows:

$$F_i = -\frac{\rho u_i u_r}{r} - \frac{2\rho v u_r}{r^2}\delta_{ir} \quad (3)$$

and $\kappa$ is expressed as follows:

$$\kappa = \frac{1}{c^2}\sum_\alpha e_{\alpha x} e_{\alpha x} = \frac{1}{c^2}\sum_\alpha e_{\alpha r} e_{\alpha r} \quad (4)$$

where $e_{\alpha i}$ is the $i$th element of the velocity vector for a particle in $\alpha$ direction, $\omega_h$ is an effective relaxation time (hydrodynamic frequency) in relation to the hydrodynamic dimensionless single relaxation time, $\tau_{h-cy}$, with the following definition:

$$\omega_h = \begin{cases} \dfrac{1}{\tau_{h-cy}}, & r = 0 \\ \dfrac{1}{\tau_{h-cy}}\left[1 + \dfrac{(2\tau_{h-cy} - 1)e_{\alpha r}\Delta t}{2r}\right], & r \neq 0 \end{cases} \quad (5)$$

In Equation (5), the definition of the hydrodynamic dimensionless single relaxation time in a cylindrical coordinate system is as follows:

$$\tau_{h-cy} = \left(\frac{\nu_{LB}}{c_s^2 \Delta t} + 0.5\right) \quad (6)$$

If we use the two-dimensional lattice ($D_2Q_9$) that shown in Figure 2, the value of $w_\alpha$ will be as follows:

$$w_\alpha = \begin{cases} \frac{4}{9} & \alpha = 0 \\ \frac{1}{9} & \alpha = 1,3,5,7 \\ \frac{1}{36} & \alpha = 2,4,6,8 \end{cases} \quad (7)$$

While $\vec{e}_\alpha$ is defined as follows:

$$\vec{e}_\alpha = \begin{cases} (0,0), & \alpha = 0 \\ \lambda_\alpha\, c \left[cos\frac{(\alpha-1)\pi}{4}, sin\frac{(\alpha-1)\pi}{4}\right], & \alpha \neq 0 \end{cases} \quad (8)$$

In the above equation, $\lambda_\alpha$denotes the following expression:

$$\lambda_\alpha = \begin{cases} 1 & \alpha = 1,3,5,7 \\ \sqrt{2} & \alpha = 2,4,6,8 \end{cases} \quad (9)$$

where $\kappa$ is a constant which takes a value of 6 for a $D_2Q_9$ lattice.

Macroscopic variables of the flow, including density and axial and radial velocity components of the fluid, are defined as follows:

$$\rho = \sum_{\alpha=0}^{8} f_\alpha \quad (10)$$

$$\rho\,.\,u_x = \sum_{\alpha=1}^{8} \vec{e}_\alpha\,.\,f_\alpha \quad (11)$$

$$\rho\,.\,u_r = \sum_{\alpha=1}^{8} \vec{e}_\alpha\,.\,f_\alpha \quad (12)$$

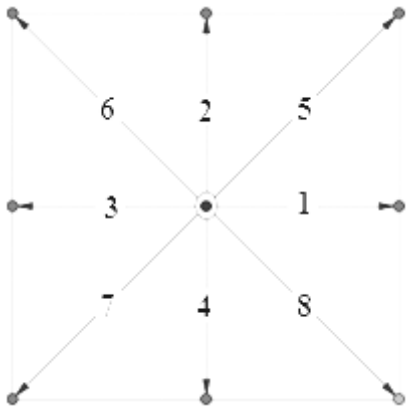


**Figure 2.** The two-dimensional 9-velocity lattice ($D_2D_9$) [20].

Local distribution function, $f_\alpha^{eq}$, is as follows:

$$f_\alpha{}^{eq} = w_\alpha \left(1 + 3\frac{e_{\alpha i}u_i}{c^2} + \frac{9}{2}\frac{e_{\alpha i}e_{\alpha j}u_i u_j}{c^4} - \frac{3}{2}\frac{u_i u_i}{c^2}\right) \quad (13)$$

Equation (1) can be solved at either of two stages: collision and streaming.

The flow field at collision stage:

$$\tilde{f}_\alpha(\vec{x}, t+\Delta t) - f_\alpha(\vec{x}, t) = -\tau_\alpha\left[f_\alpha(\vec{x}, t) - f_\alpha^{eq}(\vec{x}, t)\right] + w_\alpha\theta\,\Delta t + \frac{\Delta t}{\kappa c^2} e_{\alpha i} F_i \quad (14)$$

The flow field at the streaming stage:

Equation (14) expresses the collision stage wherein the post-collision functions, $\tilde{f}_\alpha(\vec{x}, t+\Delta t)$, are calculated at $t+\Delta t$ as functions of the local and equilibrium distribution functions at time *t*. At the streaming (propagation) stage, the distribution functions propagate across the lattice upon collision. It is worth noting that the main features of the modified model include as follows. First, the modified version has all features of the original Zhou's model [21], second, the new introduced source and force terms include no velocity gradient, making them simpler, than the existing designs [22]-[23], and third, it can easily recover the Navier-Stocks equation similar to the standard lattice Boltzmann method.

### *3.2. Axisymmetric lattice Boltzmann method for the thermal part of the flow*

Equation (16) expresses the lattice Boltzmann equation for temperature distribution function using the $D_2Q_9$ lattice arrangement for a general node inside the solution domain in a cylindrical coordinate system, as indicated in Reference [24]:

$$g_\alpha(\vec{x} + \vec{e}_\alpha\Delta t, t+\Delta t) - g_\alpha(\vec{x}, t) = -\omega_t\left[g_\alpha(\vec{x}, t) - g_\alpha^{eq}(\vec{x}, t)\right] + (1 - 0.5\,\omega_t)\,\Delta t\, S_\alpha(\vec{x}, t) \quad (16)$$

In Equation (16), given the choice of $D_2Q_9$ lattice to represent the lattice Boltzmann, the $g_\alpha(\vec{x}, t)$ denotes the temperature distribution functions along discrete velocity vector, $\vec{e}_\alpha$, at point $\vec{x}(r, x)$ and time *t*, with $\alpha = 0,1,\ldots,8$. Moreover, $g_\alpha^{eq}$ represent the equilibrium distribution functions for temperature, $S_\alpha(\vec{x}, t)$ is the source term, and $\omega_t$ is the thermal frequency, as defined in the following:

$$\omega_t = \frac{\left[1 + \left(\frac{e_{\alpha r}\,\tau_{t-cy}\,\Delta t}{r}\right)\right]}{\left(\tau_{t-cy} + 0.5\right)} \quad (17)$$

For an axisymmetric lattice Boltzmann model in a cylindrical coordinate system, the source term in Equation (16) is written as follows:

$$S_\alpha = -\frac{u_r}{r} g_\alpha^{eq} \quad (18)$$

Equation (16) can also be solved in two stages: collision and flow.

The temperature field at collision stage:

$$\tilde{g}_\alpha(\vec{x}, t+\Delta t) - g_\alpha(\vec{x}, t) = -\omega_t\left[g_\alpha(\vec{x}, t) - g_\alpha^{eq}(\vec{x}, t)\right] + (1 - 0.5\,\omega_t)\,\Delta t\, S_\alpha(\vec{x}, t) \quad (19)$$

The temperature field at the flowing stage:

$$g_\alpha(\vec{x} + \vec{e}_\alpha \Delta t, t+\Delta t) = \tilde{g}_\alpha(\vec{x}, t+\Delta t) \quad (20)$$

The required thermal equilibrium distribution functions were taken from Reference [24], as expressed in Equation (21):

$$g_\alpha^{eq} = \rho\, T\, w_\alpha \left\{1 + \frac{\vec{e}_\alpha.\vec{u}}{{c_s}^2} + \frac{1}{2}\left[\frac{(\vec{e}_\alpha.\vec{u})^2}{{c_s}^4} - \frac{\vec{u}.\vec{u}}{{c_s}^2}\right]\right\} \quad (21)$$

In this equation, $w_0 = \frac{4}{9}$, $w_{1-4} = \frac{1}{9}$, and $w_{5-8} = \frac{1}{36}$ are weighting factors in the $D_2Q_9$ model and $T$ is the fluid temperature in the lattice Boltzmann environment. Moreover, $\vec{u} = (u_x, u_r)$ denotes the macroscopic velocity vector where $u_x$ and $u_r$ represent the axial and normal components of the macroscopic velocity vector in the lattice Boltzmann environment. $c_s = \sqrt{RT}$ is the sound velocity in the lattice Boltzmann, which is equal to $c_s = \frac{1}{\sqrt{3}}$ in the $D_2Q_9$ model, with $R$ being the universal gas constant for an ideal gas.

Discrete velocity vector, $\vec{e}_\alpha$, for $\alpha$ direction is given as Equation (22).

$$\vec{e}_\alpha = \begin{cases} (0,0)\cdot c, & \alpha = 0 \\ (cos[(\alpha-1)\pi/2], \\ sin[(\alpha-1)\pi/2])\cdot c, & \alpha = 1,2,3,4 \\ (cos[(2\alpha-9)\pi/4], \\ sin[(2\alpha-9)\pi/4])\sqrt{2}\cdot c, & \alpha = 5,6,7,8 \end{cases} \quad (22)$$

where $c = \sqrt{3RT} = \frac{\Delta x}{\Delta t}$ is the lattice Boltzmann velocity with the time step $\Delta t$ and lattice step $\Delta x$. Finally, the macroscopic temperature of the fluid is determined as follows:

$$T = \frac{\sum_{\alpha=0}^{8} g_\alpha}{\left[1 + 0.5\,\Delta t \frac{u_r}{r}\right]} \quad (23)$$

The value of $\tau_{t-cy}$ in Equation (17) is a function of thermal diffusivity ($\alpha_t$), as follows:

$$\tau_{t-cy} = \left(\frac{\alpha_t}{c_s^2 \Delta t} + 0.5\right) \quad (24)$$

### 3.3. Boundary conditions

The application of boundary conditions in the lattice Boltzmann method is a relatively complex matter. This complexity stems from the fact that there is still no physical understanding of the behavior of distribution functions along the boundaries. For a general problem, there is nothing but macroscopic parameters of the flow. Therefore, it is necessary to translate this macroscopic information into the information required for the distribution function in the mesoscopic scale. There is no single methodology for performing this translation step. Inappropriate performance of this stage imposes significant impacts on not only the accuracy and validity of the subsequent numerical simulations but also stability and convergence of the lattice Boltzmann method.

#### 3.3.1. Boundary conditions

In this research, the boundary conditions proposed by Chang *et al.* [25] and Ho *et al.* [26] were utilized to determine the unknown density distribution functions along the input boundaries, lower and upper walls of the tube. This method combines known local values with a corrector.

Figure 3 shows the tube boundaries and directions of the density distribution functions along the boundaries. It is worth noting that the unknown distribution function is marked as red arrows.

Unknown distribution functions $f_1$, $f_5$, and $f_8$ at the input boundary of the tube are as follows:

$$f_1 = f_3 + \frac{2}{3}\rho\, u_r \quad (25)$$

$$f_5 = f_7 + \frac{1}{6}\rho\, u_x + \frac{1}{2}\rho\, u_r - \frac{1}{2}(f_2 - f_4) \quad (26)$$

$$f_8 = f_6 + \frac{1}{6}\rho\, u_x - \frac{1}{2}\rho\, u_r + \frac{1}{2}(f_2 - f_4) \quad (27)$$

Besides, unknown distribution functions $f_2$, $f_5$, and $f_6$ on the lower wall of the tube are as follows:

$$f_2 = f_4 \quad (28)$$

$$f_5 = f_7 - \frac{1}{2}(f_1 - f_3) \quad (29)$$

$$f_6 = f_8 + \frac{1}{2}(f_1 - f_3) \quad (30)$$

The unknown distribution functions $f_4$, $f_7$, and $f_8$ on the upper wall of the tube are as follows:

$$f_4 = f_2 \quad (31)$$

$$f_7 = f_5 + \frac{1}{2}(f_1 - f_3) \quad (32)$$

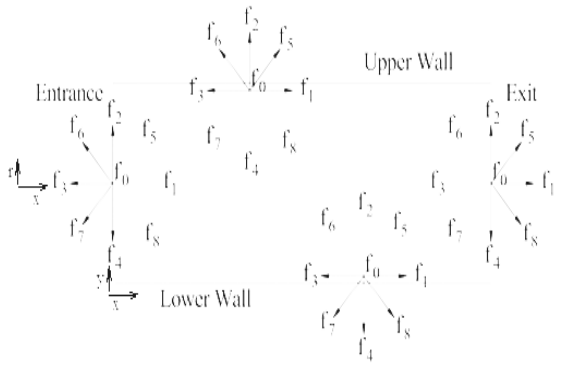


Figure 3. Mass density distribution functions at boundary points along the tube.

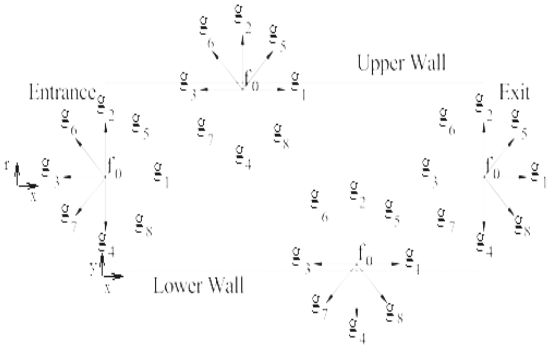


Figure 4. Temperature distribution functions at points along the tube boundary.

$$f_8 = f_6 - \frac{1}{2}(f_1 - f_3) \quad (33)$$

The vector of velocity at the output section of the tube is unknown; however, given the larger length-to-diameter ratio of the tube in this study, the velocity profile at the output section of the tube is expected to reach the fully developed state. If the output boundary of the flow field is located at $i = N$, then the values of the unknown functions $f_3$, $f_6$, and $f_7$ along such boundary can be obtained from the first-order extrapolation method proposed as follows [27]:

$$f_{3,N} = f_{3,N-1} \quad (34)$$

$$f_{6,N} = f_{6,N-1} \quad (35)$$

$$f_{7,N} = f_{7,N-1} \quad (36)$$

Moreover, to enhance the solution accuracy, one can adopt second-order extrapolation, as follows:

$$f_{3,N} = 2f_{3,N-1} - f_{3,N-2} \quad (37)$$

$$f_{6,N} = 2f_{6,N-1} - f_{6,N-2} \quad (38)$$

$$f_{7,N} = 2f_{7,N-1} - f_{7,N-2} \quad (39)$$

### *3.3.2. Boundary conditions*

The state of temperature distribution functions along the tube boundaries in a $D_2Q_9$ lattice Boltzmann model is the same as that of density distribution functions. In this research, the boundary conditions proposed in Ref. [27] were used to determine unknown particle temperature distribution functions along the input and output boundaries. To formulate unknown particle temperature distribution functions along the lower and lower walls of the tube, the boundary conditions proposed in Ref. [28] were utilized. Figure 4 shows the tube boundaries along with the directions of the density distribution functions along the boundaries. It is noteworthy that the unknown distribution functions are highlighted as red arrows.

The unknown distribution functions $g_1$, $g_5$, and $g_8$ along the tube boundary were defined as follows:

$$g_1 = T_{in}(w_1 + w_3) - g_3 \quad (40)$$

$$g_5 = T_{in}(w_5 + w_7) - g_7 \quad (41)$$

$$g_8 = T_{in}(w_8 + w_6) - g_6 \quad (42)$$

In the above equations, $T_{in}$ is the nanofluid temperature at the tube boundary, and $w_{1,3,5,6,7,8}$ are weighting factors.

In the present problem, constant heat flux was applied on the tube walls; therefore, adopting the Fourier's law at $r = \pm R$ gives:

$$-k_{nf}\frac{\partial T}{\partial r} = q'' \xrightarrow{T=g} -k_{nf}\frac{\partial g}{\partial r} = q'' \quad (43)$$

In Equation (43), $k_{nf}$ is the thermal conductivity of the nanofluid passing through the conduit, $q''$is the constant heat flux applied to the tube wall, and $g$ is the temperature distribution function. If the lower wall is located at $j = 0$, then the unknown temperature distribution functions on the lower wall of the tube can be written as follows:

$$g_3(i,0) = g_3(i,1) + \frac{q''\Delta r}{k_{nf}} \quad (44)$$

$$g_5(i,0) = g_5(i,1) + \frac{q''\Delta r}{k_{nf}} \quad (45)$$

$$g_6(i,0) = g_6(i,1) + \frac{q''\Delta r}{k_{nf}} \quad (46)$$

If the upper wall is located at $j = M$, then the unknown temperature distribution functions on the upper wall of the tube can be written as follows:

$$g_4(i,M) = g_4(i,M-1) + \frac{q''\Delta r}{k_{nf}} \quad (47)$$

$$g_7(i,M) = g_7(i,M-1) + \frac{q''\Delta r}{k_{nf}} \quad (48)$$

**Table 1.** Thermophysical properties of different phases of the nanofluid.

| Property | Solid phase [8] | Liquid phase(water)[29] |
|---|---|---|
| $k$ | $46\ \frac{W}{(\mathrm{m.K})}$ | $k_{bf} = -9.2784 \times 10^{-6} \times T_{in}^2 + 0.0021476 \times T_{in} + 0.55855$ |
| $\mu$ | --- | $\mu_{bf} = 0.1966 \times 10^{-3} \times T_{in}^2 - 0.028469 \times T_{in} + 1.4769$ |
| $\rho$ | $3890\ \frac{\mathrm{Kg}}{m^3}$ | $\rho_{bf} = -0.31429 \times 10^{-2} \times T_{in}^2 - 0.12429 \times T_{in} + 1002.2$ |
| $Pr$ | --- | $Pr_{bf} = \frac{\nu_{bf}}{\alpha_{bf}}$ |
| $c_p$ | 880 J/Kg.K | $(c_p)_{bf} = \frac{k_{bf} Pr_{bf}}{\mu_{bf}}$ |
| $\phi$ | $\phi = 0.01, 0.03, 0.05$ | --- |

$$g_8(i,M) = g_8(i,M-1) + \frac{q''\Delta r}{k_{nf}} \quad (49)$$

Given the larger length-to-diameter ratio of the tube in this study, the temperature profile at the output section of the tube is expected to reach a fully developed state, so that temperature variations in flow direction at the output boundary would be negligible. If the output boundary of the temperature field is located at *i* = *N*, then the values of the unknown functions along such boundary can be obtained from the first-order extrapolation method proposed, as follows [27]:

$$g_{3,N} = g_{3,N-1} \quad (50)$$

$$g_{6,N} = g_{6,N-1} \quad (51)$$

$$g_{7,N} = g_{7,N-1} \quad (52)$$

Moreover, to enhance the solution accuracy, one can adopt second-order extrapolation, as follows:

$$g_{3,N} = 2g_{3,N-1} - g_{3,N-2} \quad (53)$$

$$g_{6,N} = 2g_{6,N-1} - g_{6,N-2} \quad (54)$$

$$g_{7,N} = 2g_{7,N-1} - g_{7,N-2} \quad (55)$$

### *3.4. Thermophysical properties of the nanofluid*

The thermophysical properties of different phases of the nanofluid are detailed in Table 1. As can be observed in this table, density, viscosity, and thermal conductivity of the liquid phase (water) are functions of the input fluid temperature.

Pak and Cho [30] proposed temperature-independent constant values for a density of the nanofluids based on a volumetric fraction of the nanoparticles, as written in Equation (56).

$$\rho_{nf} = (1-\phi)\rho_{bf} + \phi\,\rho_p \quad (56)$$

where $\rho_{bf}$, $\rho_p$, and $\rho_{nf}$ denote the densities of the base fluid, nanoparticles, and the nanofluid, respectively, and $\phi$ is the volumetric fraction of the nanoparticles.

Similar to the density, Zhuan and Rutzel [5] proposed constant temperature-independent values for the thermal conductivity of the nanofluid as a function of the volumetric fraction of the nanoparticles, as expressed in Equation (57).

$$(\rho Cp)_{nf} = (1-\phi)(\rho Cp)_{bf} + \phi(\rho Cp)_p \quad (57)$$

Numerous models have been proposed for the viscosity of nanofluids, as reviewed by Huminic et al. [31]. In the present research, we used the model proposed by Maiga et al. [32], as written in Equation (58).

$$\mu_{nf} = (1 + 7.3\,\phi + 123\,\phi^2)\mu_{bf} \quad (58)$$

Where $\mu_{bf}$ and $\mu_{nf}$ are viscosities of the base fluid and nanofluid, respectively.

The most significant parameter for representing the enhanced thermal potential of nanofluids is their thermal conductivity. Consequently, the determination of thermal conductivity is of paramount importance in nanofluids. As reviewed by Huminic et al. [31], various models have been proposed for this purpose. In the present work, we use the model proposed by Maxwell [33], as per Equation (59):

$$k_{nf} = \left(\frac{k_p + 2k_{bf} + 2\phi(k_p - k_{bf})}{k_p + 2k_{bf} - \phi(k_p - k_{bf})}\right) \times k_{bf} \quad (59)$$

where $k_{nf}$ is the thermal conductivity of the nanofluid, $k_{bf}$ is the thermal conductivity of the base fluid, and $k_p$ is the thermal conductivity of the nanoparticles.

Thermal diffusivity and Prandtl number of the nanofluid can be calculated from the following relationship respectively [31]:

$$\alpha_{nf} = \frac{k_{nf}}{(\rho C_p)_{nf}} \quad (60)$$

$$Pr_{nf} = \frac{\nu_{nf}}{(\alpha)_{nf}} \quad (61)$$

In this problem, the solution method is that the nanofluid's thermophysical properties are calculated first. In the next step, to solve the hydrodynamic part of the flow, Equations 14 and 15 are solved by using the

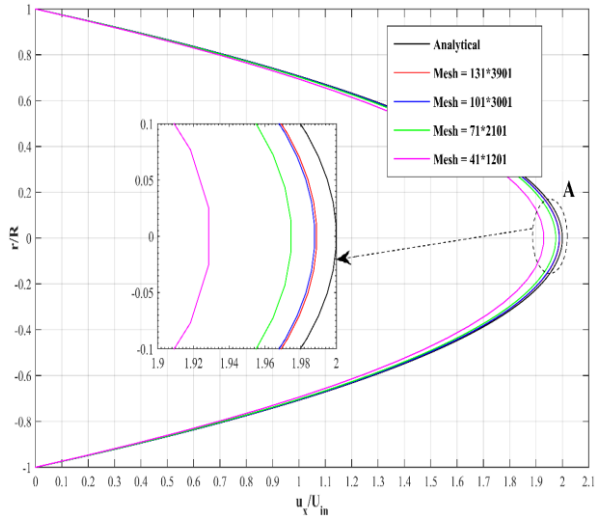


**Figure 5.** Axial dimensionless component of the velocity profile at the hydrodynamic ally developed section of the tube under different grid arrangements with respective analytic solutions.

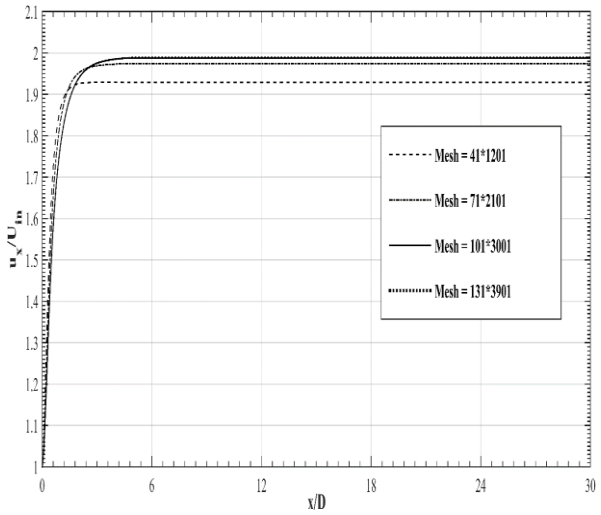


**Figure 6.** Variations of the axial dimensionless component of the velocity along the tube axis for different grid arrangements.

**Table 2**. Investigation of grid independence and validation.

| Mesh | $\frac{u_{x,max}}{U_{in}}$ | | $(\frac{x}{D})$ | |
|---|---|---|---|---|
| | Present work | Relative error% | Present work | Relative error% |
| 41×2101 | 1.9285 | 3.5756 | 4.5 | 10 |
| 71×2101 | 1.9745 | 1.2749 | 4.571 | 8.58 |
| 101×3001 | 1.9877 | 0.6144 | 4.636 | 7.28 |
| 131×3901 | 1.9889 | 0.5548 | 5.04 | 1 |

boundary conditions in Equations 25 to 39. After validating the solution, equations 19 and 20 are solved to obtain the thermal part of the flow by using the boundary conditions in Equations 40 to 55.

## 4. Grid independence and validation

In this problem, the lattice Boltzmann model with identical spatial steps along *x* and *r* directions was utilized. In order to ensure grid independence of the lattice, the problem was solved using four different lattices at Reynolds number of 100 for base fluid (water) and the following results are presented and compared.

Axial dimensionless component of the velocity profile at the hydrodynamically developed section of the tube under four different grid arrangements with respective analytic solutions are illustrated in Figure 5. According to Figure 5, the finer size, the closer would get the velocity profile to a perfect hyperbola (i.e. analytic solution).

Figure 6 depicts the variations of the axial dimensionless component of the velocity along the tube axis for different grid arrangements. On this figure, it is evident that the finer the grids, the more accurate would be the obtained location of hydrodynamic development of the flow based on the analytic solution (Table 2).

Table 2 presents an interpretation of the results demonstrated in Figures 5 and 6 for investigating the grid independence and validation of the present methodology.

A comparison between the maximum axial dimensionless velocity ($\frac{u_{x,max}}{U_{in}}$) obtained from this method to that calculated per $u_{x,max}/\left[U_{in}\left(1-\left(\frac{r}{R}\right)^2\right)\right]$ (adapted from Ref. [34]) for different grid arrangements show that the difference between the results of a 101 × 3001 lattice and a 131 × 3901 lattice is less than 0.06%, with a percent error of only 0.61% concerning the analytic solution. Moreover, comparing the hydrodynamic entrance length $(x/D)_h$ obtained from this method to that from $(x/D)_h \approx 0.05Re$ (adapted from Ref. [35]) for different grid arrangements showed that the difference between the results of a 101 × 3001 lattice and a 131 × 3901 lattice is less than 4.02%, with a percent error of 7.28% regarding the analytic solution ($(x/D)_h = 5$). This was while the coarser grids required merely one seventh of the processing time taken for the finer grids. Therefore, the 101 × 3001 lattices were chosen for solving the problem.

To ensure the validity of the results in the thermal part of the flow, variations of the Nusselt number of the base fluid (water) with Prandtl number of 5 were calculated on the tube walls. Moreover, the obtained Nusselt number was compared to that calculated by Hornbeck [36] and the percent error values are reported in Table 3. As one may observe in Figure 7, the Nusselt number was plotted in the range of $0.001 \leq x^* \leq 0.02$, and the curve of Nusselt number obtained using the present methodology reveals that the present method provides a good agreement with the Hornbeck's [36] curve of Nusselt numbers. Furthermore, Table 3 indicates that the percent relative error of the present research compared to Ref. [33] is something between 4 and 18.1%, with an average percent relative error of 9.21%.

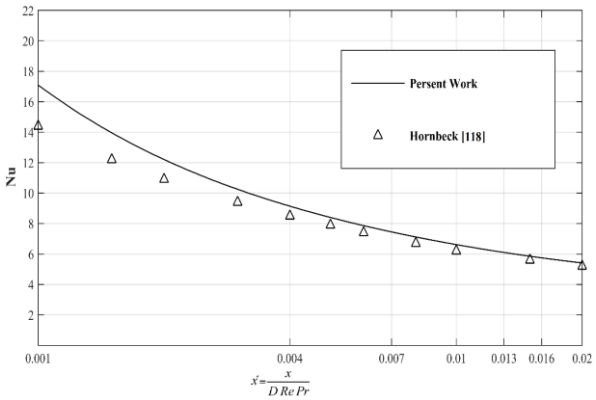


**Figure 7.** A comparison of variations of Nusselt number for the base fluid between the present solution method and Ref. [33].

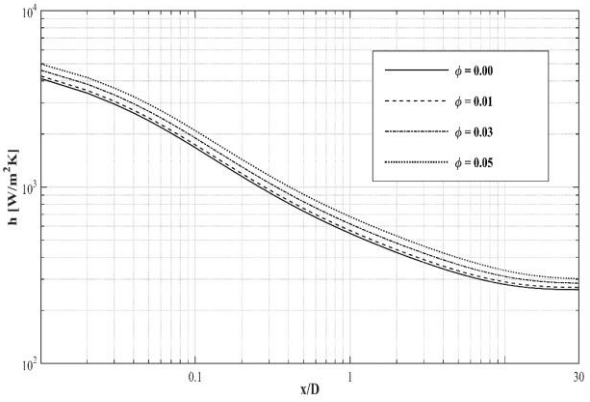


**Figure 8.** Variations of forced convection heat transfer on the lower wall of the tube at different volumetric fractions for Reynolds number of 50 and Tin = 293K.

**Table 3.** A comparison between the Nusselt number in the present research and that in Ref. [33] at different values of $x^*$.

| $x^* = \frac{x}{D\,Re\,Pr}$ | Present work | Hornbeck [33] | Relative error % |
|---|---|---|---|
| 0.001 | 17.01 | 14.4 | 18.1 |
| 0.0015 | 13.80 | 12.2 | 13.1 |
| 0.002 | 12.15 | 10.9 | 11.5 |
| 0.003 | 10.20 | 9.4 | 8.6 |
| 0.004 | 9.10 | 8.5 | 7.1 |
| 0.005 | 8.39 | 7.9 | 6.3 |
| 0.006 | 7.86 | 7.4 | 6.2 |
| 0.008 | 7.12 | 6.7 | 6.1 |
| 0.01 | 6.62 | 6.2 | 6.7 |
| 0.015 | 5.85 | 5.6 | 4.47 |
| 0.02 | 5.41 | 5.2 | 4.1 |

## 5. Results

The results are plotted in the form of diagrams of forced convection heat transfer coefficient and Nusselt number versus the ratio of the axial distance from the start of the tube to the tube height, $\frac{x}{D}$. Figures 8 – 12 show the results of the present numerical method for the water – aluminum oxide nanofluid at input temperature of 20℃ and either of four volumetric concentrations: 0% (water as base fluid), 1%, 3%, and 5%.

### *5.1. Effect of volumetric ratio of nanoparticles on forced convection heat transfer*

Figures 8 and 9 present the variations of forced convection heat transfer coefficient and Nusselt number for the water-aluminum oxide nanofluid at four volumetric concentrations, namely 0% (water as base fluid), 1%, 3%, and 5%, at Reynolds number of 50 and input temperature of 20℃. As can be observed in Figure 8, as one moves along the length of the tube, increasingly lower values of heat transfer coefficient were observed. Indeed, given the constant nature of the heat flux applied to the entire length of the tube, the tube wall temperature increases, thereby increasing the temperature difference between the fluid and the wall and hence reducing the heat transfer coefficient have occurred. In other words, the heat transfer is mainly performed at the input section of the tube, and as one moves along the tube toward the thermally developed part of the flow, the increased temperature difference between the fluid and the tube wall lowers the heat transfer coefficient. consequently, when designing cooling systems, the designer must keep in mind that the heat exchange shall occur in the thermally developed flow zone. In Figure 8, it is observed that the forced convection heat transfer coefficient increases with the nanoparticle concentration increasing. The average increase in forced convection heat transfer coefficient along the tube length ($0 \leq \frac{x}{D} \leq 30$) was found to be 3.22%, 10.52%, and 18.86% at a volumetric concentration of 1%, 3%, and 5%, respectively. The introduction of nanoparticles to the base fluid enhances the thermal conductivity of the nanofluid over the base fluid, and this contributes to increased forced convection heat transfer coefficient through the nanofluid, as compared to the base fluid.

Figure 9 depicts that the Nusselt number increases with nanoparticle concentration. Accordingly, the average increase in Nusselt number along the tube length ($0 \leq \frac{x}{D} \leq 30$) was found to be 0.30%, 1.47%, and 3.22% at a volumetric concentration of 1%, 3%, and 5%, respectively. Please note that the difference between the increases in forced convection heat transfer coefficient and Nusselt number stems from the fact that thermal conductivity appears in the denomination of the Nusselt number. Therefore, since an increase in the nanoparticle concentration translates into enhanced thermal conductivity, then the increase in the Nusselt number upon

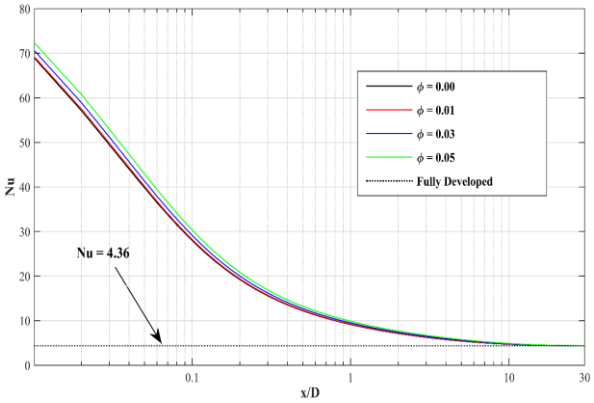


**Figure 9.** Variations of Nusselt number on the lower wall of the tube at different volumetric fractions at Reynolds number of 50 and $T_{in} = 293\ K$.

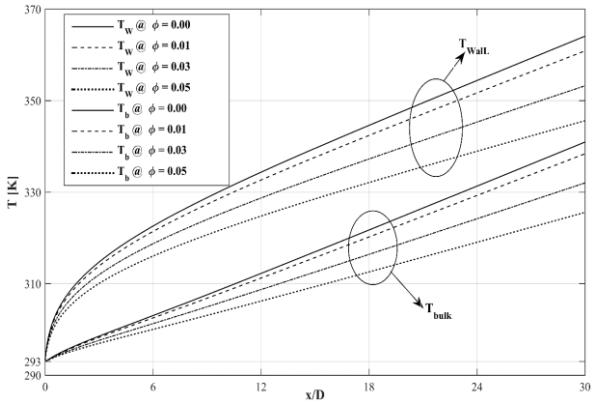


**Figure 10.** Changes in the wall temperature and bulk temperature at different volumetric fractions for Reynolds number of 50 and $T_{in} = 293\ K$.

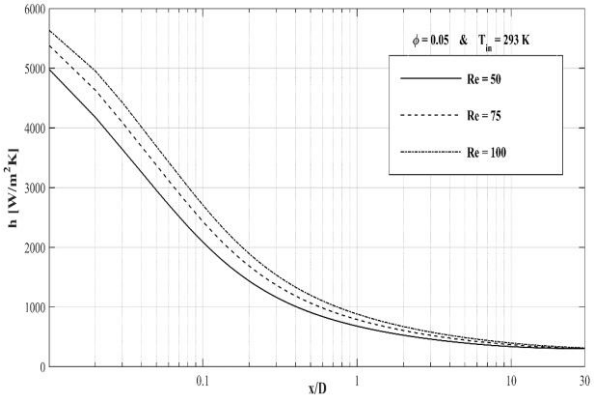


**Figure 11.** Changes in the forced convection heat transfer coefficient on the lower wall of the tube at different Reynolds numbers at a volumetric fraction of 5% and $T_{in}$ = 293 K.

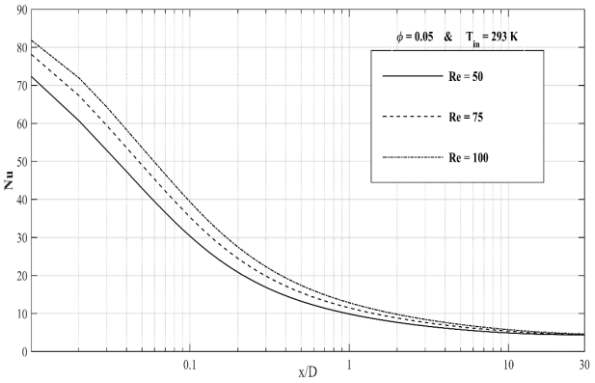


**Figure 12.** Changes in the Nusselt number on the lower wall of the tube at different Reynolds numbers at a volumetric fraction of 5% and $T_{in}$ = 293 K.

enhancing the nanoparticle concentration is somewhat lower than the respective increase in forced convection heat transfer coefficient. Figure 9 further shows the changes in the Nusselt number on the lower wall of the tube at different volumetric fractions of the nanoparticles, as compared to the analytic solution, in the fully developed section of the flow. On this basis, the value of Nusselt number as per the present numerical solution for pure water in the fully developed section was found to be 4.61, and the fact that Ref. [31] reports a Nusselt number of 4.36 for the fully developed section of the tube, the percent error is 5.68%. Moreover, the thermal development length ($\left(\frac{x}{D}\right)_t$) obtained from the present numerical solution for pure water was found to be 11.32, and since the thermal development length obtained per $\frac{\left(\frac{x}{D}\right)_t}{\left(\frac{x}{D}\right)_h} = Pr$ [31] for pure water is 11.56, the respective percent error is 2.09%.

To better understand the reason behind higher forced convection heat transfer coefficient and hence Nusselt number with increasing the volumetric concentration of nanoparticles in the base fluid, curves of changes in wall temperature and bulk temperature of the nanofluid along the tube length at four volumetric fractions (0% (base fluid, water), 1%, 3%, and 5%) are presented in Figure 10.

This figure indicates that the decrease in the tube wall temperature and balk temperature of the nanofluid, increases along the tube length, as compared to the base fluid.

## *5.2. Effect of Reynolds number on forced convection heat transfer*

Figures 11 and 12 illustrate the variations of forced convection heat transfer coefficient and Nusselt number for the water-aluminum oxide nanofluid at a volumetric concentration of 5%, input temperature of 20℃, and three different Reynolds numbers, namely 50, 75, and 100. Figure 11 shows that an increase in Reynolds number adds to the forced convection heat transfer coefficient. Accordingly, the average increase in forced convection heat transfer coefficient along the tube length ($0 \leq \frac{x}{D} \leq 30$) was found to be 18.86%, 20.32%, and 21.36% at Reynolds numbers of 50, 75, and 100, respectively.

Figure 12 indicates that an increase in Reynolds number increases the Nusselt number. Accordingly, the average increase in Nusselt number along the tube length ($0 \leq \frac{x}{D} \leq 30$) at a volumetric concentration of 5% was found to be 3.22%, 4.48%, and 5.38% at Reynolds numbers of 50, 75, and 100, respectively. As can be observed in the figures,

the forced convection heat transfer coefficient and Nusselt number increased with increasing Reynolds number.

### *5.3. Effect of input temperature on forced convection heat transfer*

In this research, the forced convection heat transfer coefficient and Nusselt number of the studied nanofluid were calculated at two different input temperatures to evaluate the capability of the nanofluid for relative enhancement of forced convection heat transfer coefficient and Nusselt number at different temperatures. To analyze the impact of volumetric concentration of the nanoparticles on forced convection heat transfer coefficient and Nusselt number, Tables 4 and 5 represent the percent changes in forced convection heat transfer and Nusselt number of the nanofluid, respectively, as compared to the base fluid for different volumetric fractions of the nanofluid in several axial distances. The figure indicates that, at any axial distance and for a given volumetric fraction of the nanoparticles, forced convection heat transfer and Nusselt number increase with decreasing the input temperature.

Moreover, in order to analyze the impact of Reynolds number on the forced convection heat transfer coefficient and Nusselt number, Tables 6 and 7 represent the percent changes in forced convection heat transfer and Nusselt temperature increases the forced convection heat transfer number of the nanofluid, respectively, as compared to the base fluid at the same Reynolds number for several axial distances. The results indicate that a decrease in input coefficient and Nusselt number, as compared to the base fluid, at any axial distance for a given Reynolds number. To investigate the effect of input temperature on the relative increase in forced convection heat transfer coefficient and Nusselt number, average percent increases in forced convection heat transfer coefficient and Nusselt number for a volumetric fraction of 5% and the entire length of the tube ($0 \leq \frac{x}{D} \leq 30$) is presented in Table 8. Corresponding results to the starting segment of the tube ($0.1 \leq \frac{x}{D} \leq 7$) are tabulated in Table 9. The presented results imply that the water-aluminum oxide nanofluid with a concentration of 5% at an input temperature of 15℃ (288K) exhibits higher heat transfer and Nusselt number than those of the same nanofluid at an input temperature of 20℃ (293K). Moreover, the results revealed that such

**Table 4.** Percent changes in forced convection heat transfer coefficient at different volumetric fractions and Reynolds number of 50 for different axial distances and two input temperatures.

| $x/D$ | $\phi = 1\%$ h | | $\phi = 3\%$ h | | $\phi = 5\%$ h | |
|---|---|---|---|---|---|---|
| | $T_{in} = 293\ K$ | $T_{in} = 288\ K$ | $T_{in} = 293\ K$ | $T_{in} = 288\ K$ | $T_{in} = 293\ K$ | $T_{in} = 288\ K$ |
| 0.11 | 3.85 | 3.94 | 13.52 | 13.63 | 25.09 | 25.45 |
| 1 | 3.76 | 3.85 | 13.12 | 13.43 | 24.44 | 24.75 |
| 3.52 | 3.64 | 3.73 | 12.62 | 12.71 | 23.39 | 23.66 |
| 7.06 | 3.47 | 3.48 | 11.74 | 11.84 | 21.52 | 21.80 |
| 11.30 | 3.24 | 3.28 | 10.71 | 10.79 | 19.39 | 19.58 |

**Table 5.** Percent changes in Nusselt number at different volumetric fractions and Reynolds number of 50 for different axial distances and two input temperatures.

| $\frac{x}{D}$ | $\phi = 1\%$ Nu | | $\phi = 3\%$ Nu | | $\phi = 5\%$ Nu | |
|---|---|---|---|---|---|---|
| | $T_{in} = 293\ K$ | $T_{in} = 288\ K$ | $T_{in} = 293\ K$ | $T_{in} = 288\ K$ | $T_{in} = 293\ K$ | $T_{in} = 288\ K$ |
| 0.11 | 0.91 | 0.10 | 4.22 | 4.32 | 8.62 | 8.9 |
| 1 | 0.82 | 0.91 | 3.86 | 4.14 | 3.40 | 8.32 |
| 3.52 | 0.70 | 0.79 | 3.40 | 3.48 | 7.15 | 7.38 |
| 7.06 | 0.54 | 0.55 | 2.59 | 2.68 | 5.52 | 5.76 |
| 11.30 | 0.32 | 0.36 | 1.65 | 1.72 | 3.68 | 3.83 |

**Table 6.** Percent changes in forced convection heat transfer coefficient at different Reynolds numbers at a fixed volumetric fraction of 5, as compared to the base fluid, for different axial distances and two input temperatures.

| $x/D$ | $Re = 50$ | | $Re = 75$ | | $Re = 100$ | |
|---|---|---|---|---|---|---|
| | h | | h | | h | |
| | $T_{in} = 293\ K$ | $T_{in} = 288\ K$ | $T_{in} = 293\ K$ | $T_{in} = 288\ K$ | $T_{in} = 293\ K$ | $T_{in} = 288\ K$ |
| 0.11 | 25.09 | 25.45 | 25.25 | 25.65 | 25.34 | 25.71 |
| 1 | 24.44 | 24.75 | 24.60 | 25.94 | 24.69 | 25.01 |
| 3.52 | 23.39 | 23.66 | 23.78 | 24.09 | 24.14 | 24.32 |
| 7.06 | 21.52 | 21.80 | 22.88 | 23.11 | 23.46 | 23.78 |
| 11.30 | 19.39 | 19.58 | 21.31 | 21.54 | 22.40 | 22.61 |

**Table 7.** Percent changes in Nusselt number at different Reynolds numbers at a fixed volumetric fraction of 5, as compared to the base fluid, for different axial distances and two input temperatures.

| x/D | Re = 50 | | Re = 75 | | Re = 100 | |
|---|---|---|---|---|---|---|
| | Nu | | Nu | | Nu | |
| | $T_{in} = 293$ K | $T_{in} = 288$ K | $T_{in} = 293$ K | $T_{in} = 293$ K | $T_{in} = 288$ K | $T_{in} = 293$ K |
| 0.11 | 8.62 | 8.93 | 8.76 | 9.10 | 8.84 | 9.16 |
| 1 | 8.06 | 8.32 | 8.21 | 8.48 | 8.28 | 8.54 |
| 3.52 | 7.15 | 7.38 | 8.49 | 7.74 | 7.80 | 7.94 |
| 7.06 | 5.52 | 5.7593 | 6.71 | 6.90 | 7.21 | 7.47 |
| 11.30 | 3.68 | 3.83 | 5.34 | 5.53 | 6.30 | 6.46 |

**Table 8.** A comparison between the average percent increase in forced convection heat transfer coefficient and Nusselt number at two different Reynolds number when $0 \leq \frac{x}{D} \leq 30$ for a volumetric fraction of 5% at two different temperatures.

| $Re$ | $\overline{h}$ | | $\overline{Nu}$ | |
|---|---|---|---|---|
| | $T_{in} = 293\ K$ | $T_{in} = 288\ K$ | $T_{in} = 293\ K$ | $T_{in} = 288\ K$ |
| 50 | 18.86 | 19.13 | 3.22 | 3.35 |
| 75 | 20.32 | 20.64 | 4.48 | 4.66 |
| 100 | 21.36 | 21.72 | 5.39 | 5.60 |

**Table 9.** A comparison between the average percent increase in forced convection heat transfer coefficient and Nusselt number at two different Reynolds number when $0.1 \leq \frac{x}{D} \leq 7$ for a volumetric fraction of 5% at two different temperatures.

| $Re$ | $\overline{h}$ | | $\overline{Nu}$ | |
|---|---|---|---|---|
| | $T_{in} = 293\ K$ | $T_{in} = 288\ K$ | $T_{in} = 293\ K$ | $T_{in} = 288\ K$ |
| 50 | 23.33 | 25.01 | 7.09 | 7.75 |
| 75 | 23.90 | 25.63 | 7.59 | 8.29 |
| 100 | 24.16 | 25.91 | 8.82 | 8.54 |

an increase is even more pronounced along the starting segment of the tube.

The larger increase in heat transfer for the nanofluid at lower input temperature can be linked to the higher viscosity gradient at lower temperatures. This may lead to increased viscosity gradient inside the tube, thereby contributing to the nanoparticle migration and Brownian motions and hence heat transfer. Therefore, when designing cooling systems with low-temperature thermal fields, the use of water-aluminum oxide nanofluid rather than pure water can further add to heat transfer.

## Conclusion

In this research, to investigate the flow and forced convection heat transfer through homogeneous water/$Al_2O_3$ nanofluid inside a horizontal tube, the axisymmetric lattice Boltzmann method was used. The heat transfer was performed along with a steady-state flow under a laminar flow regime. Uniform velocity and temperature were assumed at the input section, constant heat flux was considered on the walls of the conduit, and the fully developed condition for the velocity and temperature was assumed at the output section of the tube. The effects of the volumetric concentration of the nanoparticles and input temperature to the tube on thermal parameters of the flow were investigated at different Reynolds numbers. According to the obtained results, the following conclusions were drawn:

- The results indicated that the utilized axisymmetric lattice Boltzmann method is capable of simulating the flow and heat transfer with good accuracy.
- The amounts of increase in forced convection heat transfer coefficient and Nusselt number of the nanofluid were functions of the volumetric concentration of the nanoparticles; so that with increasing the volumetric concentration of the nanoparticles, the amounts of forced convection heat transfer coefficient and Nusselt number of the nanofluid over those of the base fluid increased.
- With increasing Reynolds number, forced convection heat transfer coefficient and Nusselt number increase over the base fluid and nanofluid.
- With decreasing the input temperature, forced convection heat transfer coefficient and Nusselt number increase over the base fluid and nanofluid for any axial distance and a given Reynolds number; Moreover, with decreasing the input temperature, forced convection heat transfer coefficient and Nusselt number increase over the base fluid and nanofluid for any axial distance and a volumetric fraction of the nanoparticles.
- Average increases in the values of the heat transfer coefficient and Nusselt number of the water-aluminum oxide nanofluid were larger at lower input temperatures; Moreover, this increase was even more pronounced in the starting segment of the tube.
- The average increase in forced convection heat transfer coefficient of the nanofluid at input temperature of 15℃ was 7.24% larger than that at the input temperature of 20℃.
- At lower input temperature to the tube, percent increases in forced convection heat transfer coefficient and Nusselt number increase with Reynolds number.

## Acknowledgements

Authors would like to thank the Vice-chancellor for research, Shahid Chamran University of Ahvaz (Grant number: SCU.EM99.376).

## Conflict of interest

The authors declare no conflict of interest.

## References

[1] Das, S.K., Choi, S.U. and Patel, H.E., 2006. Heat transfer in nanofluids—a review. Heat transfer engineering, 27(10), pp.3-19.

[2] Wang, X.Q. and Mujumdar, A.S., 2008. A review on nanofluids-part I: theoretical and numerical investigations. Brazilian Journal of Chemical Engineering, 25(4), pp.613-630.

[3] Eastman, J.A., Choi, U.S., Li, S., Thompson, L.J. and Lee, S., 1996. Enhanced thermal conductivity through the development of nanofluids (No. ANL/MSD/CP-90462; CONF-961202-94). Argonne National Lab., IL (United States).

[4] Lee, S., Choi, S.S., Li, S.A. and Eastman, J.A., 1999. Measuring thermal conductivity of fluids containing oxide nanoparticles.

[5] Xuan, Y. and Roetzel, W., 2000. Conceptions for heat transfer correlation of nanofluids. International Journal of heat and Mass transfer, 43(19), pp.3701-3707.

[6] Wen, D. and Ding, Y., 2004. Experimental investigation into convective heat transfer of nanofluids at the entrance region under laminar flow conditions. International journal of heat and mass transfer, 47(24), pp.5181-5188.

[7] Shah, R.K., 1975, December. Thermal entry length solutions for the circular tube and parallel plates. In Proceedings of 3rd national heat and mass transfer conference, 1, pp.11. Indian Institute of Technology Bombay.

[8] Noghrehabadi, A. and Pourrajab, R., 2016. Experimental investigation of forced convective heat transfer enhancement of γ-Al 2 O 3/water nanofluid in a tube. Journal of

Mechanical Science and Technology, 30(2), pp.943-952.
[9] Hassanzadeh, R., Ozbek, A. and Bilgili, M., 2016. Analysis of alumina/water nanofluid in thermally developing region of a circular tube. Thermal Engineering, 63(12), pp.876-886.
[10] Nourgaliev, R.R., Dinh, T.N., Theofanous, T.G. and Joseph, D., 2003. The lattice Boltzmann equation method: theoretical interpretation, numerics and implications. International Journal of Multiphase Flow, 29(1), pp.117-169.
[11] Xuan, Y. and Yao, Z., 2005. Lattice Boltzmann model for nanofluids. Heat and mass transfer, 41(3), pp.199-205.
[12] Kefayati, G.R., Hosseinizadeh, S.F., Gorji, M. and Sajjadi, H., 2011. Lattice Boltzmann simulation of natural convection in tall enclosures using water/SiO2 nanofluid. International Communications in Heat and Mass Transfer, 38(6), pp.798-805.
[13] Javaherdeh, K. and Ashorynejad, H.R., 2014. Magnetic field effects on force convection flow of a nanofluid in a channel partially filled with porous media using Lattice Boltzmann Method. Advanced Powder Technology, 25(2), pp.666-675.
[14] Sidik, N.A.C. and Mamat, R., 2015. Recent progress on lattice Boltzmann simulation of nanofluids: A review. International Communications in Heat and Mass Transfer, 66, pp.11-22.
[15] Cheng, P., Gui, N., Yang, X., JiyuanTu and Jiang, S., 2018. Application of lattice Boltzmann methods for the multiphase fluid pipe flow on graphical processing unit. The Journal of Computational Multiphase Flows, 10(3), pp.109-118.
[16] Goodarzi, M., D'Orazio, A., Keshavarzi, A., Mousavi, S. and Karimipour, A., 2018. Develop the nano scale method of lattice Boltzmann to predict the fluid flow and heat transfer of air in the inclined lid driven cavity with a large heat source inside, Two case studies: Pure natural convection & mixed convection. Physica A: Statistical Mechanics and Its Applications, 509, pp.210-233.
[17] Nazari, M. and Kayhani, M.H., 2016. A Comparative Solution of Natural Convection in an Open Cavity using Different Boundary Conditions via Lattice Boltzmann Method. Journal of Heat and Mass Transfer Research, 3(2), pp.115-129.
[18] Bahoosh, R., Jafari, M. and Bahrainian, S.S., 2019. GDL construction effects on distribution of reactants and electrical current density in PEMFC. Journal of Heat and Mass Transfer Research, 6(2), pp.105-116.
[19] Shomali, M. and Rahmati, A., 2020. Numerical analysis of gas flows in a microchannel using the Cascaded Lattice Boltzmann Method with varying Bosanquet parameter. Journal of Heat and Mass Transfer Research, 7(1), pp.25-38.
[20] Zhou, J.G., 2011. Axisymmetric lattice Boltzmann method revised. Physical review E, 84(3), p.036704.
[21] Zhou, J.G., 2008. Axisymmetric lattice Boltzmann method. Physical Review E, 78(3), p.036701.
[22] Guo, Z., Han, H., Shi, B. and Zheng, C., 2009. Theory of the lattice Boltzmann equation: lattice Boltzmann model for axisymmetric flows. Physical Review E, 79(4), p.046708.
[23] Li, Q., He, Y.L., Tang, G.H. and Tao, W.Q., 2010. Improved axisymmetric lattice Boltzmann scheme. Physical Review E, 81(5), p.056707.
[24] Li, Q., He, Y.L., Tang, G.H. and Tao, W.Q., 2009. Lattice Boltzmann model for axisymmetric thermal flows. Physical Review E, 80(3), p.037702.
[25] Chang, C., Liu, C.H. and Lin, C.A., 2009. Boundary conditions for lattice Boltzmann simulations with complex geometry flows. Computers & Mathematics with Applications, 58(5), pp.940-949.
[26] Ho, C.F., Chang, C., Lin, K.H. and Lin, C.A., 2009. Consistent boundary conditions for 2D and 3D lattice Boltzmann simulations. Computer Modeling in Engineering and Sciences (CMES), 44(2), p.137.
[27] Javaherdeh, K. and Ashorynejad, H.R., 2014. Magnetic field effects on force convection flow of a nanofluid in a channel partially filled with porous media using Lattice Boltzmann Method. Advanced Powder Technology, 25(2), pp.666-675.
[28] Mohamad, A.A., 2011. Lattice Boltzmann Method, London, Springer.
[29] Pourrajab R., 2013, Experimental investigation of forced convective heat transfer through channel with nanofluids. Msc Thesis, Shahid Chamran University, Ahvaz, Iran.
[30] Pak, B.C. and Cho, Y.I., 1998. Hydrodynamic and heat transfer study of dispersed fluids with submicron metallic oxide particles. Experimental Heat Transfer an International Journal, 11(2), pp.151-170.
[31] Huminic, G. and Huminic, A., 2012. Application of nanofluids in heat exchangers: A review. Renewable and Sustainable Energy Reviews, 16(8), pp.5625-5638.

[32] Maiga, S.E.B., Palm, S.J., Nguyen, C.T., Roy, G. and Galanis, N., 2005. Heat transfer enhancement by using nanofluids in forced convection flows. International journal of heat and fluid flow, 26(4), pp.530-546.
[33] Maxwell, J.C., 1873. A treatise on electricity and magnetism, Oxford: Clarendon Press.
[34] Bejan, A., 2013. Convection heat transfer. John wiley & sons.
[35] Incropera, F.P., Lavine, A.S., Bergman, T.L. and DeWitt, D.P., 2007. Fundamentals of heat and mass transfer. Wiley.
[36] Hornbeck, R.W., 1966, January. AN ALL-NUMERICAL METHOD FOR HEAT TRANSFER IN INLET OF A TUBE. In MECHANICAL ENGINEERING, 88(1), pp. 76. 345 E 47TH ST, NEW YORK, NY 10017: ASME-AMER SOC MECHANICAL ENG.